Research Square

Preprints are preliminary reports that have not undergone peer review.
They should not be considered conclusive, used to inform clinical practice,
or referenced by the media as validated information.

Photocatalytic Degradation of Eosin Yellow dye by Ti doped NiO Nanoparticles and their Bioactivity Performance

Mazhar Ali

mazharali9060@gmail.com

Bacha Khan University Charsadda (24420)

Muhammad Tajdar Jandal

Xi'an Jiaotong University

Muhammad Owais

Bacha Khan University Charsadda (24420)

Hamad Ali

Wali Khan University

Zahid Ali

University of Malakand Chakdara

Khalid Saeed

Bacha Khan University Charsadda (24420)

Research Article

Keywords: Ti doped NiO NPs, XRD, Photodegradation, Kinetic Study, Eyosin Yellow

Posted Date: March 24th, 2026

DOI: https://doi.org/10.21203/rs.3.rs-8986527/v1

License: This work is licensed under a Creative Commons Attribution 4.0 International License.
Read Full License

Additional Declarations: No competing interests reported.

Version of Record: A version of this preprint was published at Water, Air, & Soil Pollution on July 22nd, 2026. See the published version at https://doi.org/10.1007/s11270-026-09734-4.

Photocatalytic Degradation of Eosin Yellow dye by Ti doped NiO Nanoparticles and their Bioactivity Performance

Mazhar Ali[1]*, Muhammad Tajdar Jandal[2], Muhammad Owais[1], Hamad Ali[3], Zahid Ali[4] and Khalid Saeed[1]**

[1]Department of Chemistry, Bacha Khan University Charsadda, Charsadda, Khyber Pakhtunkhwa, Pakistan

[2]School of Chemistry, Xi'an Jiaotong University, Suzhou (710018), China

[3]Department of Physics Abdul Wali Khan University (23200) Mardan, Khyber Pakhtunkhwa, Pakistan

[4]Department of Physics, University of Malakand Chakdara, Dir Lower (18800), Khyber Pakhtunkhwa, Pakistan

Corresponding author:

email: mazharali9060@gmail.com; **khalidkhalil2002@yahoo.com; khalidsaeed@bkuc.edu.pk

Abstract

Nickel oxide (NiO) and Titanium doped NiO nanoparticles (NPs) were prepared via co-precipitation method. The successful doping of Ti to the NiO and undope NiO NPs were confirmed by powerful characterization techniques such as SEM, EDX, FTIR, XRD and UV-visible spectroscopy. SEM indicated that NiO NPs has irregularly spherical shaped particles while Ti doped NiO NPs has pore interceded texture and more agglomerated. EDX shows the better composition of both NPs. The XRD analysis demonstrates the crystalline structure of NiO and Ti doped NiO NPs and having size of 52.34 and 55.11 nm. FTIR peaks confirmed better preparation of both NPs in the range from 100-500 cm^{-1}. The optical band gap of NiO is 3.6 eV while Ti doped NiO has 3.3 eV. After 75 minutes of irradiation time, photocatalytic degradation studies under UV irradiation showed 96 and 84% Eosin yellow (EY) dye degradation by Ti doped NiO and undope NiO NPs, respectively. Further parameters were also performed for photodegradation of EY dye like effect of catalyst dosage, pH, concentration of dye and activity of recycled catalysts. Additionally, the kinetic study demonstrates that EY dye degradation study was significantly obey Pseudo-first order kinetics as compared to Pseudo-second order kinetics. Furthermore antibacterial activity of NiO and Ti doped NiO NPs were also identified.

Key words: Ti doped NiO NPs; XRD; Photodegradation; Kinetic Study; Eyosin Yellow

Introduction

Many noxious wastes such as agricultural, domestic waste and industrial effluents contain inorganic and organic contaminants. The toxicity and persistency of these pollutants makes them detrimental to both humans and the environment whenever they are released (Heath and Davis 2008). Complex chemical molecules called dyes are used as colorants in various industries, containing printing, food, leather, fabrics, drugs etc. Up to 10% of utilized colors are present in wastewater that these industries release into aquatic systems (Zhang & Webster 2009). Approximately 800,000 ton of dyes are produced annually worldwide, with 10–15% of that amount continuously released into the aquatic environment (Zada et al., 2017). These dyes include Methylene blue, Congo red, Bromophenol blue, Bromothymol blue, Eosin yellow etc. To remove colors from aqueous solutions biological, physical and chemical methods were employed, including flocculation, ozonisation, adsorption, precipitation, reverse osmosis and ultra-filtration (Saeed et al., 2017). Additionally, it was stated that the photocatalytic degradation method is the most promising method for treating wastewater due to its benefits over conventional methods, which include rapid oxidation, the absence of polycyclic products and the ability to oxidize contaminants down to the parts per billion (ppb) levels (Saeed & Khan 2017). The most sophisticated of these uses is the photocatalytic degradation ability of NPs. Due to their great surface area, low corrosion and chemical stability metals and metal oxides make ideal heterogeneous photocatalysts. It has been reported that various metals and metal oxide nanoparticles can photodegrade organic contaminants. For instance, silver nanoparticles can photodegrade methyl orange dye when exposed to sunlight. Organic dyes with various chromopore sizes are photodegraded using TiO_2 nanoparticles. The synthesis of nanoparticles on supporting materials can enhance the photocatalytic capabilities of metals and metal oxides

(Saeed et al., 2016). Degradation is currently a sophisticated technique for organic dye decolonization. There are three types of degradation: photodegradation, thermodegradation and biodegradation. Photodegradation has become a popular method for breaking down organic dyes. The hydroxyl radical, which is produced during the advanced oxidation process, can oxidize a variety of organic molecules without producing sludge. A photocatalyst is utilized in photodegradation to perform dye photocatalytic processes. Organic dyes degrade in photodegradation process because the light energy absorbed by semiconductor more than or equal to the energy gap, producing positive holes (Sato et al., 1993). The creation of innovative nanostructured metal oxide materials has drawn more interest in recent years. Nickel oxide (NiO) is most widely used transition metal oxides for a variety of functions. Because of wide band gap like 3.6 eV to 4.0 eV, highly chemical stable and having excellent optical and electrical properties (Molla et al., 2004; Chen et al., 2006) has gained a lot of interest in many applications, including fuel cells, catalysts, electrochromic films, gas sensors (Purushothaman & Muralidharan 2009), anodes of organic LEDs (Liu et al., 2008), magnetic resources and thermoelectric equipment (Wang et al., 2002). Air-calcination of $NiCl.H_2O$ produced NiO NPs with a diameter of ten to fifteen nanometer; yet, the SEM image raises a challenging topic regarding the agglomeration of nanoparticles. Using surfactant-mediated method (Tao & Wei 2004; Lenggoro et al., 2003) produced NiO nanocrystalline particles with an average diameter in nm range. However, the TEM morphology presented that the NiO NPs had not evenly distributed (Wang et al., 2002), but with addition of other dopent materials (Cai et al., 2017), the average particle diameter was decreases. Numerous alternative strategies, containing low-pressure spray pyrolysis (Carney et al., 2006), surfactant-interceded method (Boschloo et al., 1999), simple liquid phase process (Dey et al., 2018) and other ways have been performed for the preparation

of NiO NPs. Ti doped NiO nanoparticles were created here via the co-precipitation chemical pathway, which is based on a solution procedure, one of several controlled synthesis techniques. Doping is a practical and efficient method for altering a nanomaterial's optical, electrical, magnetic and structural characteristics and properties (Dooley et al., 1994). In present work NiO and Ti doped NiO NPs were used as photocatalyst for degradation of EY dye in aqueous medium.

Materials and methods

Materials

Nickel chloride ($NiCl_2$), Titanium chloride ($TiCl_2$), Nitric acid (HNO_3) and sodium hydroxide (NaOH) were purchased from Sigma-Aldrich. Eosin Yellow (EY) dye was also provided by Sigma-Aldrich. All the chemicals were analytical grade and used as such without any further purification.

Preparation of Undope Nickel Oxide Nanoparticles

The NiO NPs were prepared by getting 50 mL $NiCl_2$ (0.2 M) solution and then adding dropwise NaOH solution (0.4 M) until the solution pH became basic. The reaction mixture was continuously stirred for 4 h at 70 ^{O}C. After given reaction time, the mixture was cooled and NPs were separated via filtration. The nanoparticles were cleansed with deionized water till the pH became neutral and then oven-dried for further use.

Preparation of Titanium Doped NiO NPs

Titanium doped Nickel oxide NPs were prepared by getting 50 mL $NiCl_2$ (0.2 M) solution and 0.02 M solution of$TiCl_2$. Then added 0.4 M sodium hydroxide solution dropwise until the pH of the solution became basic. The solution mixture was stirred continuously at 70 ^{0}C for 4 h. After

specific time the mixture was cooled and NPs were separated via filtration. The NPs were cleansed with deionized H_2O till the pH became neutral and then oven-dried for further utilization.

Photodegradation of EY Dye

The undope NiO and Ti-doped NiO nanoparticles were used as photocatalysts for the degradation of EY dye. 10 mL EY (45 ppm) solution and 0.006 g of both NPs were taken separately in beakers, and then kept in the dark for 20 min to achieve maximum adsorption–desorption equilibrium between dye and undope NiO and Ti doped NiO NPs. The samples were then placed under the UV light for various irradiation times (15, 30, 45, 60 and 75 min) with continuous stirring. After the completion of a particular irradiation time, the NPs were separated from the reaction mixture via configuration (time = 10 min and rpm = 1200). The photodegradation of EY dye was studied via UV/VIS spectrophotometer (UV-1800, Shimadzu, Japan). The percent photodegradation of given dye in aqueous medium was determined by the following equation:

$$\text{Degradation rate (\%)} = \left(\frac{C_0 - C}{C_0}\right) \times 100$$

$$\text{Degradation rate (\%)} = \left(\frac{A_0 - A}{A_0}\right) \times 100$$

Where "C_o"denoted the initial dye concentration, "C" is the pesticide concentration after UV irradiation. "A_0" represent the initial absorbance and "A" denoted the dye after UV irradiation. Five different parameters were applied on the basis of their effect.

Antimicrobial activity

Disk diffusion method

Using the agar diffusion cup plate method, the antibacterial activity of NiO and Ti-doped NiO nanoparticles was tested against E. coli. This was accomplished by preparing and using agar

media. The control was ciprofloxacin. NiO and Ti-doped NiO nanoparticles weighing approximately 0.1 mg each were precisely weighed and dissolved in 1 millilitre of distal water. Two sterile petri dishes were filled halfway with the properly prepared Luria agar medium, which was then left for approximately an hour to gel evenly. Following gelling, 50µl of each E. coli strain was added to the petri dishes, which were then evenly distributed using a spreader and tagged appropriately. The sensitivity test against the pathogenic microorganisms was conducted using the well diffusion method. Using a sterile instrument, wells of 7 mm in diameter were created. Following receipt, 50µl of each E. coli strain was added to the petri dishes, which were then evenly distributed using a spreader and tagged appropriately. The sensitivity test against the pathogenic microorganisms was conducted using the well diffusion method. A sterile cork borer was used to create wells in each petri dish that were 7 mm in diameter. The wells were half-filled with a concentration of 100 µg/ml of each NiO and Ti-doped NiO nanoparticle. For a whole day, the petri plates were incubated at 370C. Millimetres (mm) were used to measure the zone of inhibition.

Minimum inhibitory method

The antibacterial activity of synthesised NiO and Ti-doped NiO nanoparticles was assessed using the conventional microdilution method. This technique establishes the lowest concentration of NiO and Ti-doped NiO nanoparticles that prevent bacterial growth. This method made use of a disposable test tube. After adding both solutions, the tubes were cultured for 24 to 37 days. Following the preparation of a suspension of 2 mg/ml of NiO and Ti doped NiO nanoparticles by sonication in distilled water, 60 µL of each complex—aside from the negative control—was added to each tube using a two-fold method. Following the addition of particles, bacteria (60 um) were added to each tube, excluding the negative control. After that, these tubes were incubated at

37 ºC for 24 hours. Following a 24-hour incubation period, the turbidity of the bacterial growth was assessed in order to determine the MIC values.

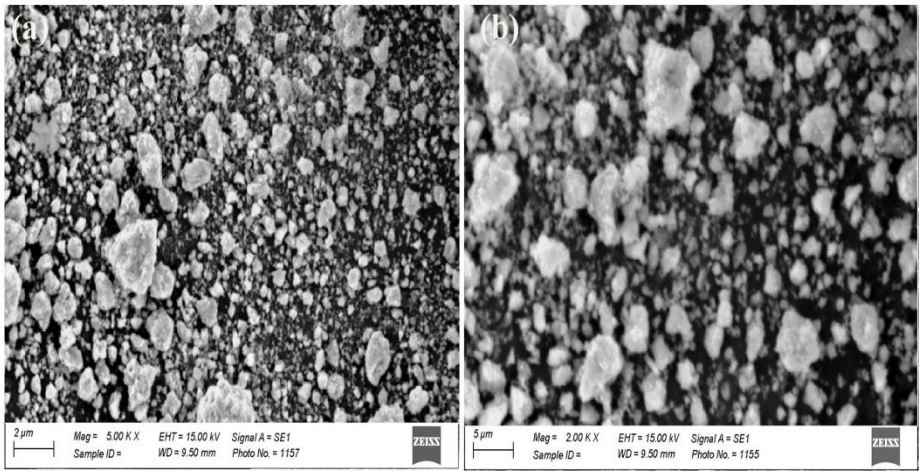
Characterization

The prepared Undoped NiO NPs and Ti doped NiO NPs were characterized via SEM (JEOL JSM-IT 100-Japan), EDX (JEOL JSM-IT 100-Japan), XRD (Model JEOL-300 analyzer) and FT-IR (PerkinElmer spectrophotometer).

Results and discussion

Morphological study

Fig. 1 shows the surface morphology performed through scanning electron microscopy (SEM) images of undoped NiO and Ti doped NiO nanoparticles. The consequences presented that some of the particles have irregular spherical shape and in agglomerated form. It was monitored that many larger NPs may be featured to NiO NPs due to their high surface tension have the ability to agglomeration (Aliahmada et al., 2014) as demonstrated in figure 1 (a and b). The average size of NiO and Ti doped NiO NPs were observed from SEM images is in nanometer range, respectively. Figure 1 (c, d) the surface morphology of the Ti doped NiO composed of aggregated particles with different size distribution. The surface morphology of the Ti doped NiO presented that the Ni particles were well captured with Ti (Mohammed et al., 2021).



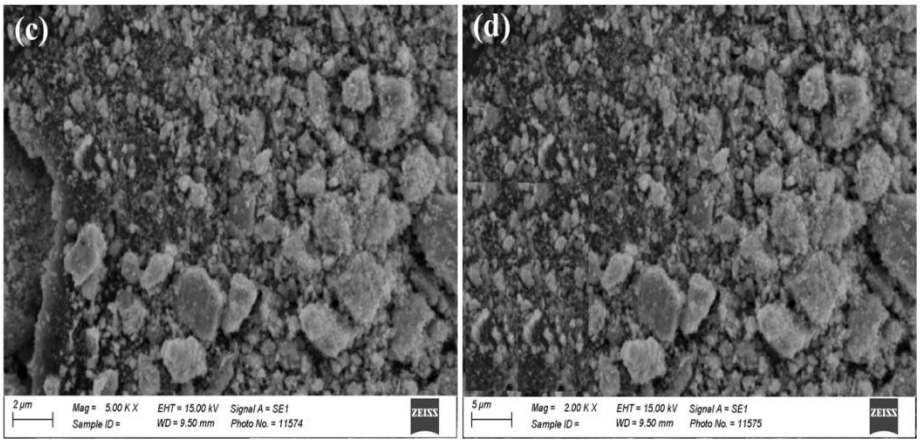


Fig.1 SEM Micrographs of (a,b) NiO NPs and (c,d) Ti doped NiO NPs

EDX Analysis

Figure 2 represents the elemental composition of undope NiO and Ti doped NiO NPs on the basis of weight % and atomic%. EDX spectra (Fig. 2a) show that the NPs contain Oxygen, Nickel and Chlorine. The weight% of O, Ni and Cl were 39.92, 56.34 and 3.74% while atomic% was 43.89, 54.02 and 2.09%, respectively. The EDX spectra (Fig. 2b) of Ti doped NiO NPs contain O, Ni and titanium and their weight% is 69.56, 29.06, 0.58 and 0.12%, and atomic% of 75.65, 23.72, 0.04 and 0.28%, respectively. The Cl was precursor slat impurities, which might be not completely eradicated during the preparation of undope NiO NPs.

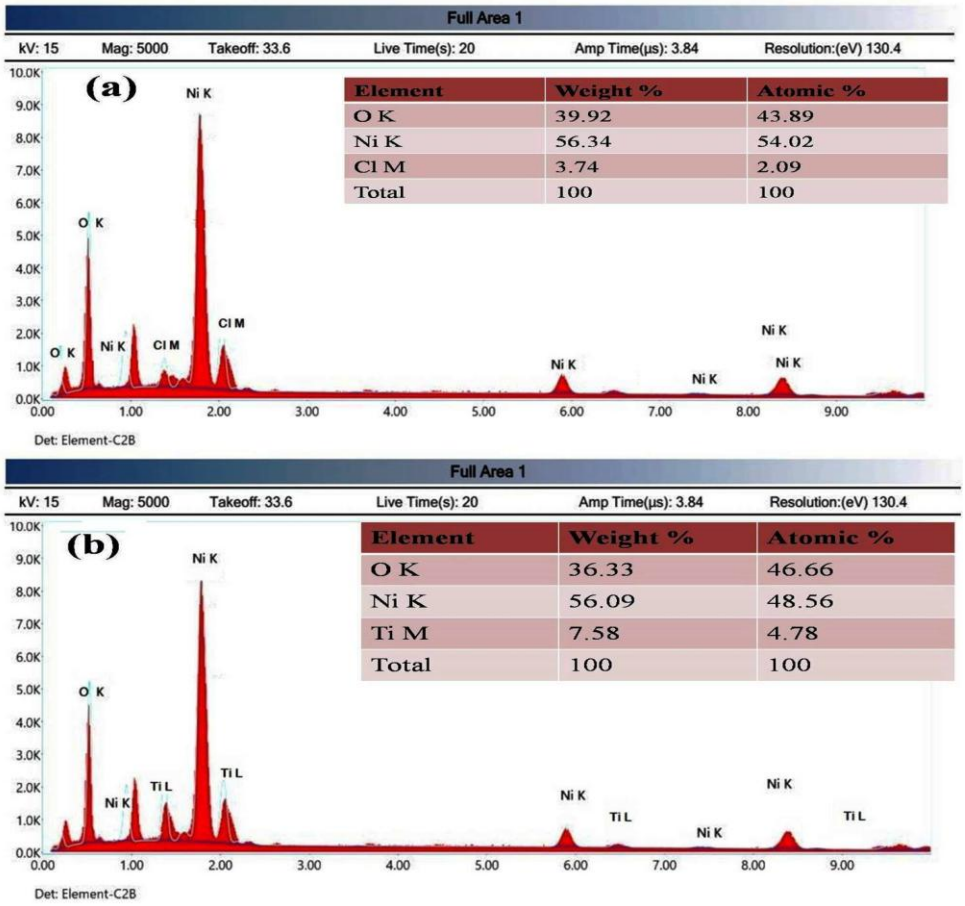


Fig.2 EDX patterns of (a) undope NiO NPs and (b) Ti doped NiO NPs

FTIR Analysis

Figure 3 shows the FTIR spectra of Undope NiO and Ti doped NiO nanoparticles. The spectra presented two characteristic peaks at 3450 cm^{-1} and 3490 cm^{-1}, which were associated to the stretching and bending modes of the hydroxyl vibration owing to the presence of physically absorbed water (Sharma & Lee 2016). The peaks at 1454 cm^{-1} and 1116 cm^{-1} belong to characteristic absorption peaks of oxide groups and NiO stretching frequencies respectively (Devi et al., 2010). Furthermore peaks at 1655 cm^{-1} and 1645 cm^{-1} are due to the bending mode (H–O–H) of the H_2O molecule of chemically prepared undope NiO NPs (Helan et al., 2016). Also the peaks at 602 and 683 cm^{-1} in lower frequencies presented the Ti–O and O–Ti–O bonding (Kumar et al., 2019). It was declared that Ti were will doped in NiO NPs.

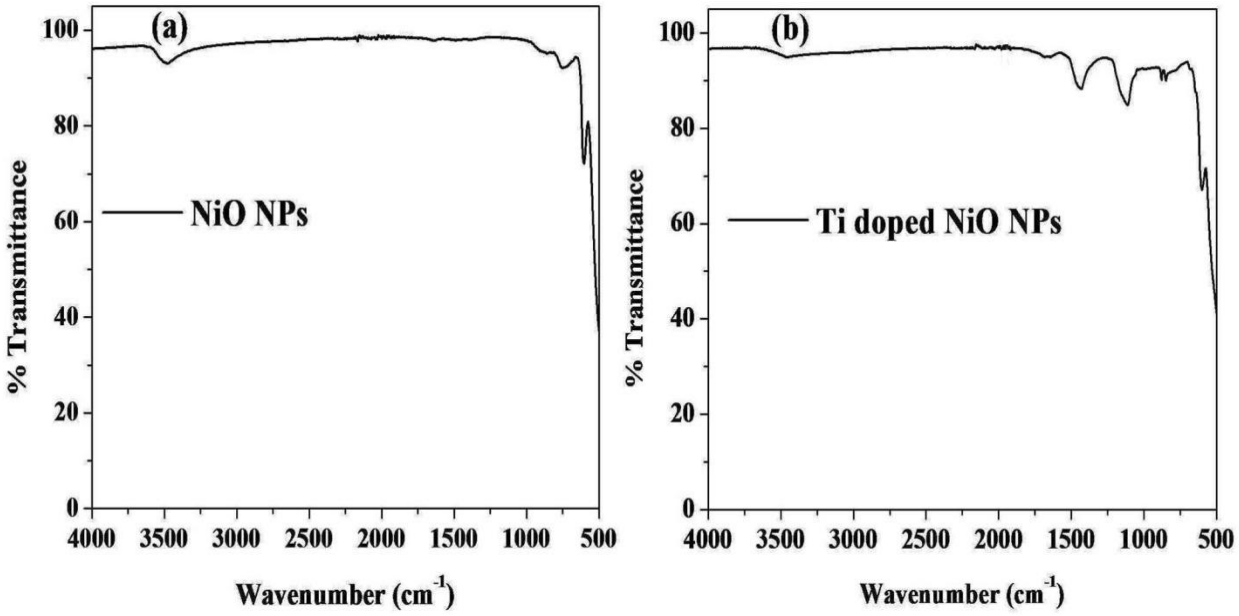


Fig.3 FTIR spectra of (a) undope NiO NPs and (b) Ti doped NiO NPs.

Band Gap Analysis

The optical band gap of NiO and Ti doped NiO NPs were identified from the recorded optical characterization data analyzed through UV/Vis absorption spectrophotometer (Kianfar et al., 2016). We can calculate the band gap energy (Eg) by using Tauc's plot. The linear portion of the plots of $(\alpha hv)^2$ against the photon energy (hü) is used to approximate the optical band gap energy (Eg). These findings suggest that, when exposed to visible light, the photocatalytic degradation activity of Ti-doped NiO should be significantly higher than that of undope NiO. According to figure 4(a), the bandgap of the synthesised NiO particles was determined to be 3.6 eV using the Tauc plot based on UV-Vis spectroscopy. As shown in figure 4(b), the band gap energy of Ti-doped NiO was lowered to 3.3eV (Rajesh et al., 2008; Shifu et al., 2009).

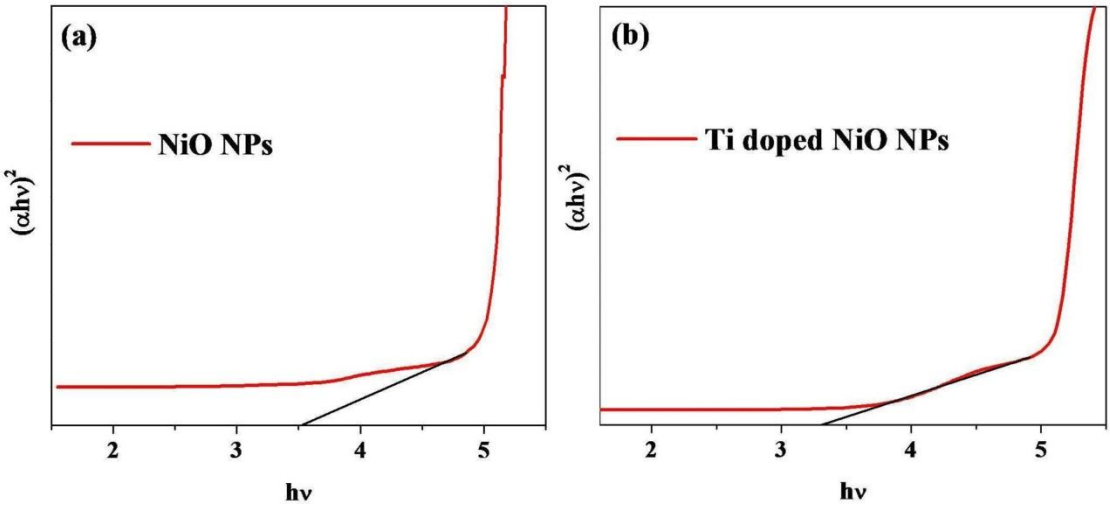


Fig. 4 The optical band gap of (a) undope NiO and (b) Ti doped NiO NPs.

XRD Analysis

The XRD pattern of undope NiO and Ti doped NiO NPs were shown in figure 5. The characteristic peaks were observed at 2θ = 78°, 42°, 62°, 37.2°, 62.7° and 75.3° indicating the NiO crystalline structure (Ramesh et al., 2021) displayed in figure 5 (a). As seen in figure 5(b), the rutile phase of Ti was represented by the major XRD peaks at 2θ values of 36.7°, 38.7° and 53.8°, whereas the anatase phase of Ti was indicated by the peaks at 25.5°, 37.9°, 48.0°, 55.1°, and 62.7°. The crystallite sizes of the undope NiO NPs and Ti-doped NiO NPs were calculated by using the Scherrer's formulae to be 55.11 and 52.34 nm, respectively (Tharwat et al.,2016).

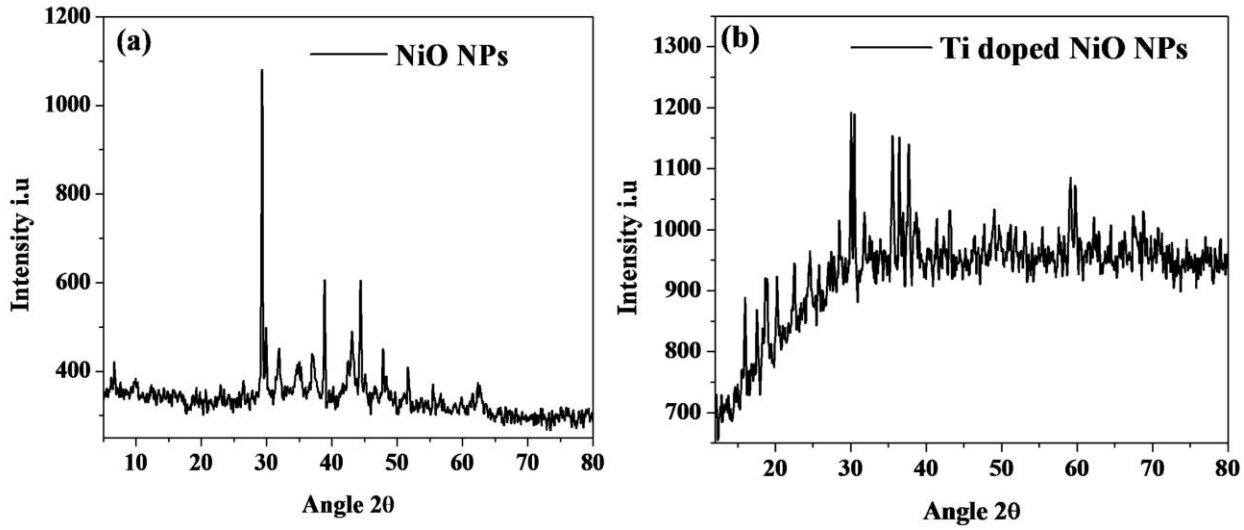


Fig. 5 XRD patterns of (a) undope NiO NPs and (b) Ti-doped NiO NPs.

Photodegradation of EY Dye by Undope NiO and Ti Doped NiO NPs

The photocatalytic degradation of Eosin Yellow (EY) dye under UV light irradiation was systematically investigated using undoped NiO NPs and Ti doped NiO NPs in an aqueous medium over varying irradiation intervals. The progress of EY dye degradation was monitored by tracking the relative intensity changes in its characteristic UV–Vis absorption peak at 517 nm. As illustrated in Figures 5a and 5b, the absorbance intensity steadily decreased with prolonged UV exposure, indicating progressive dye degradation. Quantitative analysis, depicted in figure 6c, revealed a significantly enhanced photocatalytic performance of Ti-doped NiO NPs compared to undoped NiO NPs. Specifically, undoped NiO achieved approximately 26% degradation of EY dye within 15 minutes, which increased to 84% after 75 minutes of irradiation. In contrast, Ti doped NiO exhibited a superior degradation efficiency, removing about 47% of EY dye at 15 minutes and reaching up to 96% degradation after 75 minutes. These results highlight the beneficial effect of Ti doping on NiO NPs, markedly improving their photocatalytic activity for efficient EY dye degradation under UV light.

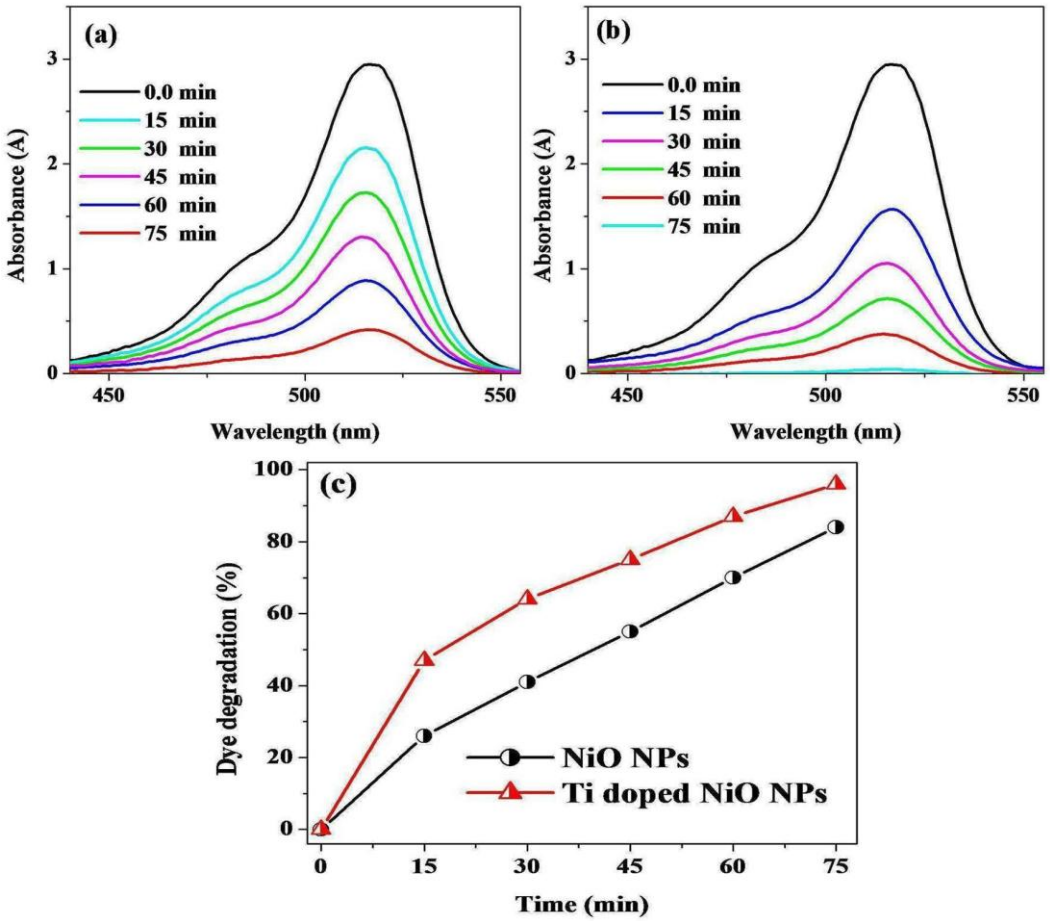


Fig. 6 UV/VIS spectra of EY dye by (a) undope NiO, (b) Ti doped NiO NPs and (c) % degradation of EY dye by NiO and Ti doped NiO NPs.

The proposed mechanism for photocatalytic degradation process facilitated by the Ti doped NiO heterostructure involves four fundamental steps: photoexcitation, oxygen ion absorption, water ionization and superoxide protonation. Upon exposure to light, the semiconductor photocatalyst generates electron-hole pair, initiating simultaneous oxidation and reduction reactions at its surface (Sharma & Lee 2016), as represented by Eqs. (7) and (8). The proposed photocatalytic mechanism for Ti doped NiO can be summarized as follows:

1. **Photoexcitation:**

$$Ti/NiO + hv \rightarrow Ti/NiO(h^{+}_VB + e^{-}_CB)$$

2. **Oxygen Ion Absorption:**

$TiO/NiO(e^-_CB) + O_2 \rightarrow TiO/NiO + \bullet O_2^-$

3. **Water Ionization:**

$H_2O \rightarrow H^+ + OH^-$

4. **Superoxide Protonation:**

$^{\bullet}O_2^- + H^+ \rightarrow {}^{\bullet}HO_2$

5. **Hydroperoxyl Radical Conversion:**

$Ti/NiO(e^-_CB) + {}^{\bullet}HO_2 + H^+ \rightarrow H_2O_2$

6. **Oxidation of Dye Molecules:**

$TiO/NiO(h^+_VB) + Dye \rightarrow$ Mineralization products (CO_2, H_2O, HA, etc.)

During the photocatalytic degradation, the primary byproducts include mineral acids (HA), where 'A' corresponds to the $-COO^-$ group derived from the nonmetal substituents of the dye molecules (Bashira et al., 2019). This comprehensive mechanism elucidates the synergistic role of Ti doped NiO in enhancing charge separation and facilitating reactive oxygen species generation, thereby driving efficient dye mineralization. General schematic mechanism of photodegradation of dyes by photocatalysts was shown in figure 7.

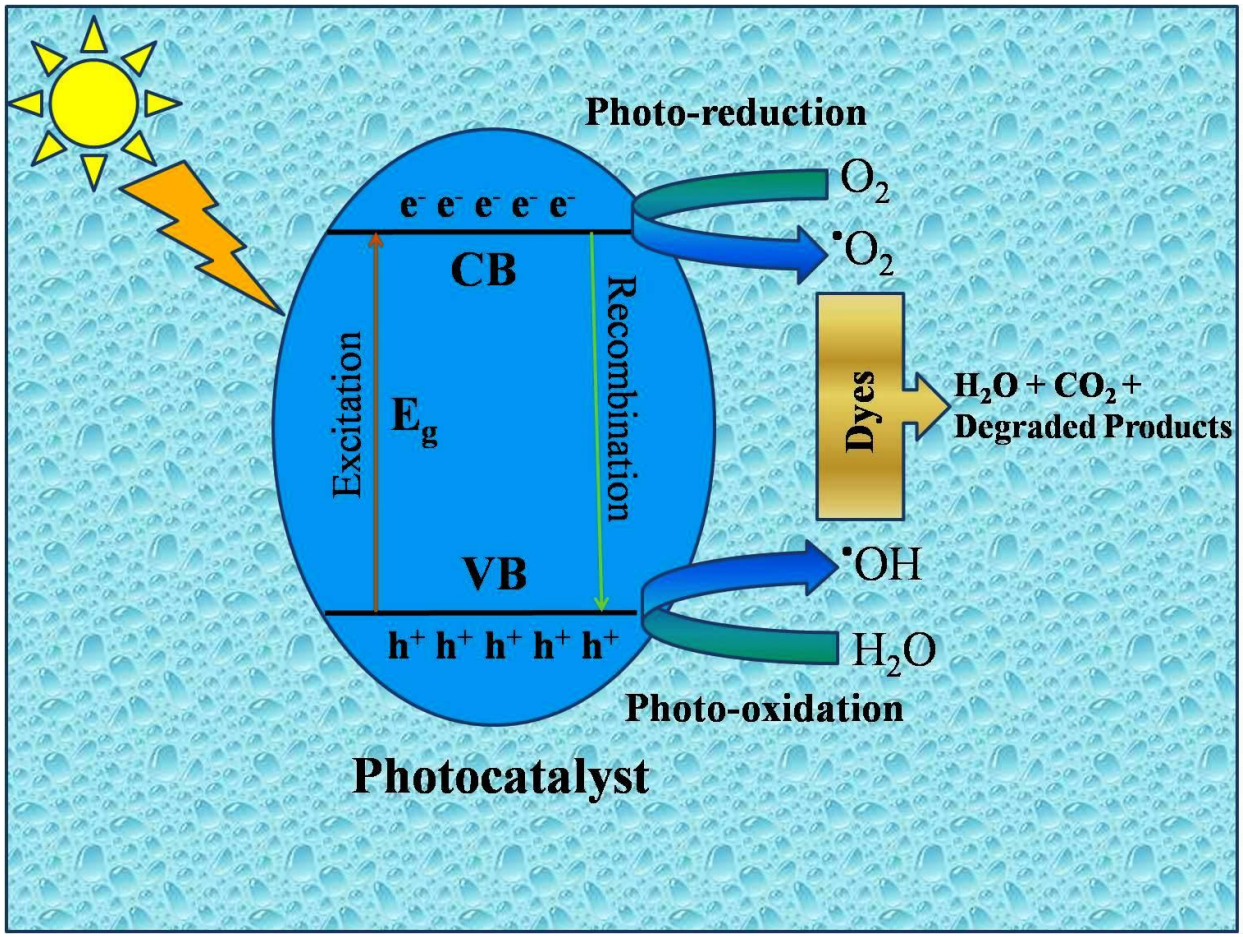


Fig.7 Schematic mechanism of photodegradation of EY dye.

Catalyst dosage effect

The influence of photocatalyst dosage on photocatalytic performance was scientifically investigated by varying the amount of photocatalyst dose (0.003, 0.006, 0.009, 0.012 and 0.015 g) while maintaining a constant irradiation time of 45 minutes and an EY dye concentration of 45 ppm. Figures (8 a and b) shows the UV–Vis absorption spectra of EY dye before and after UV irradiation in the presence of undoped NiO NPs and Ti-doped NiO NPs, respectively. The data clearly demonstrate that increasing the photocatalyst dosage significantly enhances the rate of photodegradation. Specifically, at 0.003 g loading, undoped NiO and Ti-doped NiO achieved approximately 15% and 32% dye degradation, respectively. At the highest dosage of 0.015 g,

degradation efficiencies increased markedly to 79% for undoped NiO and 88% for Ti-doped NiO as shown in figure 8 (c). This improvement in photodegradation with increasing nanoparticle loading is attributed to the greater photon absorption capacity, which promotes more efficient generation of reactive species and thus accelerates the photocatalytic degradation process.

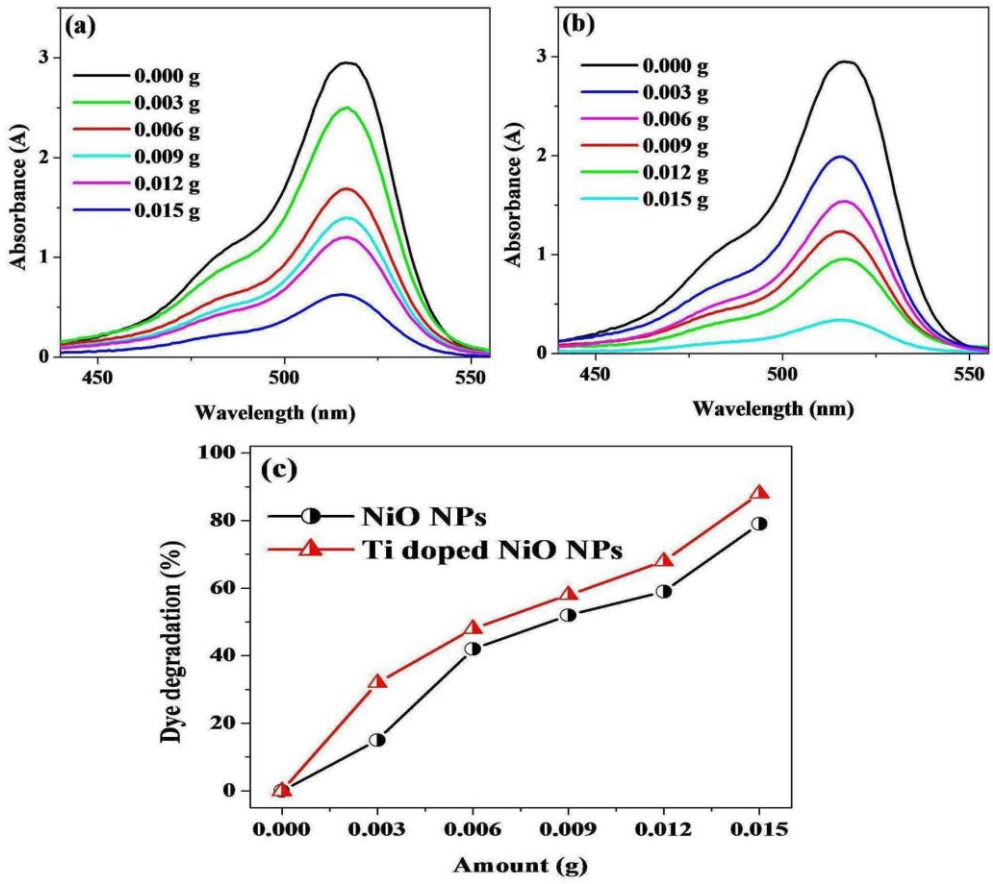


Fig.8 UV/VIS spectra of EY dye by (a) undope NiO, (b) Ti doped NiO NPs and (c) % degradation of EY dye by NiO and Ti doped NiO NPs.

Dye Concentration effect

Industrial dyeing and related processes release colored effluents at varying concentrations; therefore, the effect of dye concentration on photocatalytic degradation was systematically examined using EY dye at concentrations of 15, 30, 45, 60 and 75 ppm. The irradiation time (45 min) and catalyst dosage (0.006 g) were kept constant throughout the experiments. Figures 9 (a

and b) illustrate the UV–Vis absorption spectra and corresponding degradation percentages of EY dye, respectively, revealing that the highest photodegradation efficiency occurred at the lowest dye concentration and progressively declined with increasing initial dye concentration. As shown in figure 9 (c) at 15 ppm, undope NiO and Ti doped NiO nanoparticles achieved degradation efficiencies of 64% and 73%, respectively. In contrast, at 75 ppm, the degradation efficiencies decreased significantly to 24% for NiO and 33% for Ti doped NiO NPs. This decline in photodegradation rate at higher dye concentrations is attributed to the competitive adsorption of dye molecules on the catalyst surface, which impedes the generation of hydroxyl radicals and reduces overall photocatalytic activity.

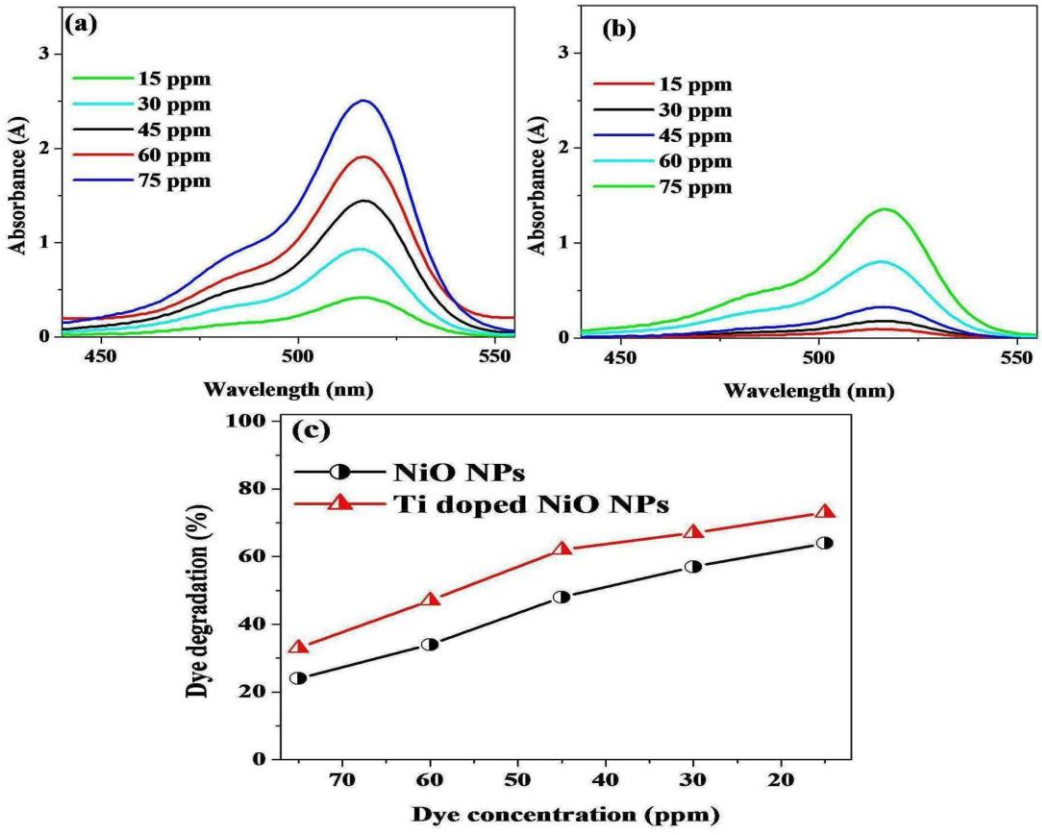


Fig. 9 UV/VIS spectra of EY dye by (a) undope NiO, (b) Ti doped NiO NPs and (c) % degradation of EY dye by NiO and Ti doped NiO NPs.

Effect of pH

The pH of the sample solution plays a vital role in photodegradation because the industries release the pollutants at different pH. The pH also affects the surface charges of the photocatalysts (Dhatshanamurthi et al., 2015). The effect of pH solution was studied in the range of pH 2–10 at a constant concentration of dye, catalyst dosage (0.006 g), and irradiated time of 45 min. At pH 10 maximum degradation were taken place. Figure 10 (a) and (b) shows the UV/Vis spectra and %degradation of EY dye at various pH. The results presented that at pH 10 NiO and Ti-doped NiO NPs degraded 56 and 82% EY dye, respectively. While at pH 2 NiO and Ti doped NiO degraded EY dye 21% and 49%, respectively as shown in Figure 10 (c).

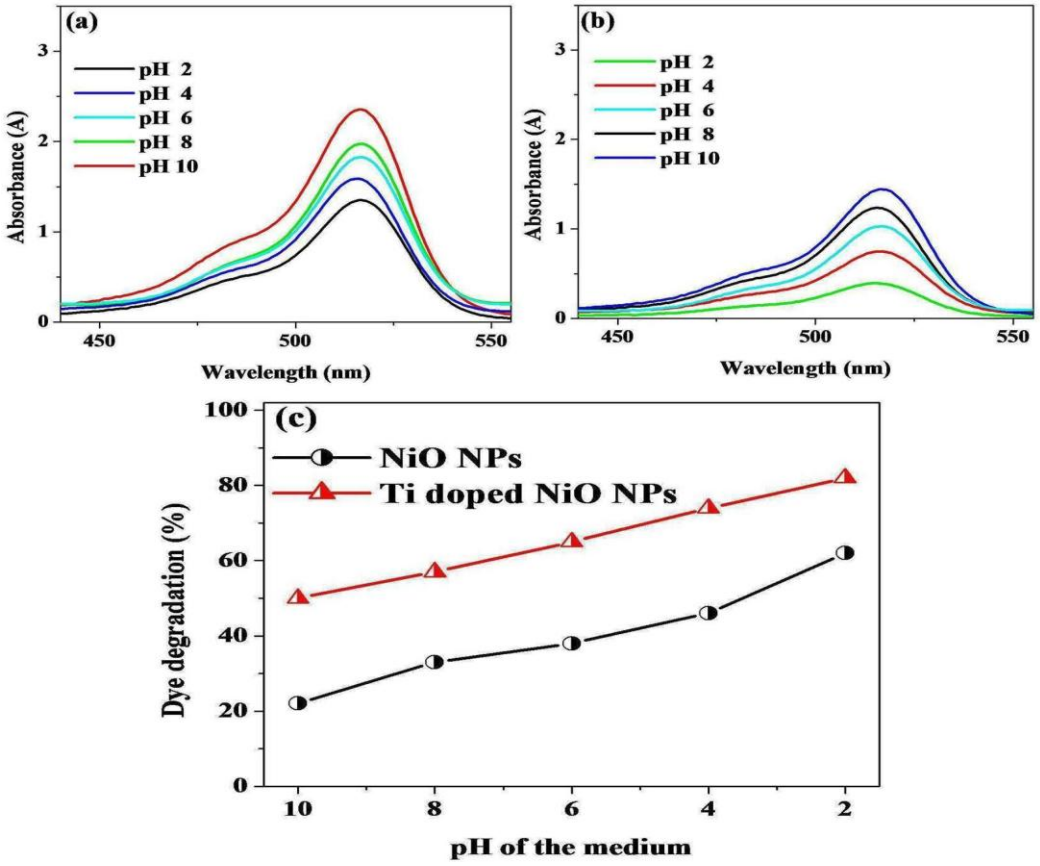


Fig.10 UV/VIS spectra of EY dye by (a) undope NiO, (b) Ti doped NiO NPs and (c) % degradation of EY dye by NiO and Ti doped NiO NPs.

Recycled catalyst effect

Figure 11 (a) and (b) shows UV/Vis spectra of EY dye degradation by recovered NiO and Ti/NiO NPs. It was found that both types of recovered catalysts also degraded the dye but their degradation ability was less than the original catalysts. It has declared that NiO NPs and Ti doped NiO NPs degraded 8% and 22% EY dye in 15 min while 22 and 51% within 75 min, respectively. Figure 11 (c) shows the percent degradation of EY dye by recovered catalysts.

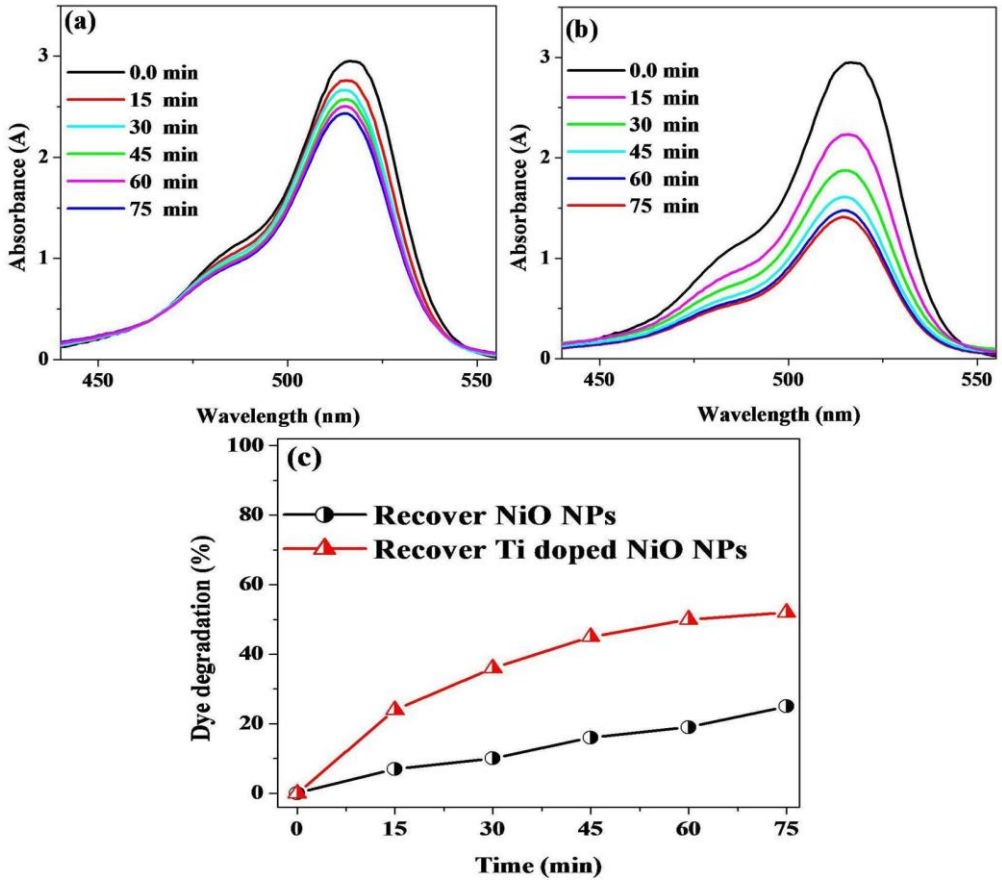


Fig. 11 UV/VIS spectra of EY dye by (a) undope NiO, (b) Ti doped NiO NPs and (c) % degradation of EY dye by NiO and Ti doped NiO NPs.

Kinetic study

In order to determine the kinetics of nanomaterials at various times at constant pH and dosage (0.006 g 10 mL^{-1}), pseudo-first order (PFO) and pseudo-second order (PSO) kinetic models were

investigated. The correlation coefficient (R^2) value was used to assess the models appropriateness (Lindaa et al., 2016). Figures 12 (a) and (b) displayed the correlation coefficient (R^2) values of pseudo-first order kinetics for undope NiO NPs and Ti doped NiO NPs were 0.96781 and 0.92295, respectively. Similarly, the R^2 values of pseudo-second-order as shown in figure 13 (a) and (b) for undope NiO NPs and Ti doped NiO NPs were 0.89016 and 0.76506, respectively (Shalini et al., 2014; Ahsan et al., 2022). Similarly, in present study the photodegradation process follows a pseudo-first-order kinetic model due to R^2 values close to 1, It provides a better fit to the degradation of several organic pollutants/dyes by undope NPs and dope NPs.

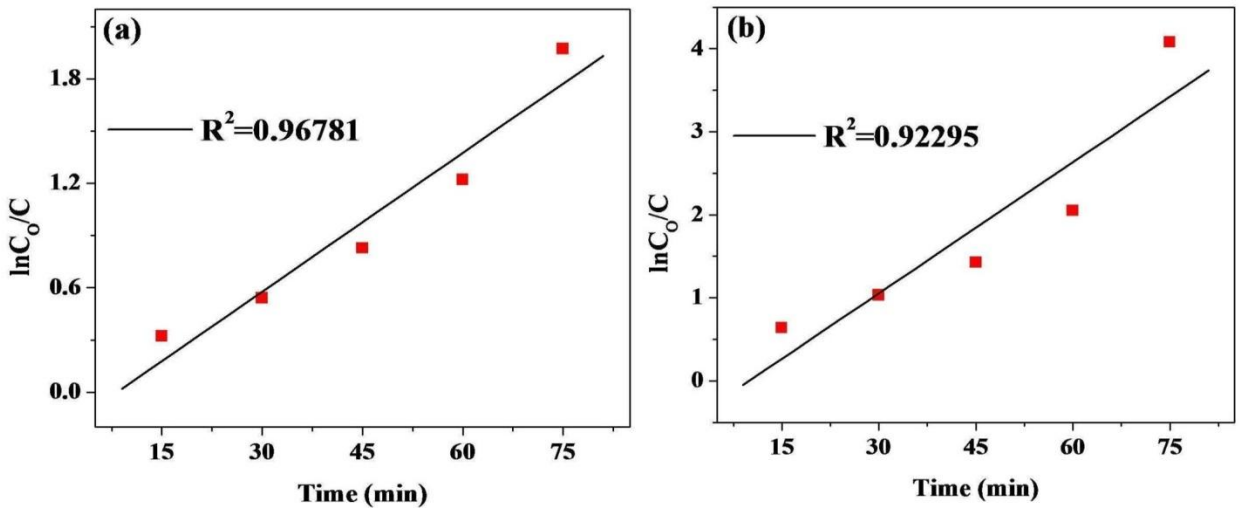


Fig. 12 Pseudo-first order kinetics of (a) Undope NiO NPs (b) Ti-doped NiO NPs

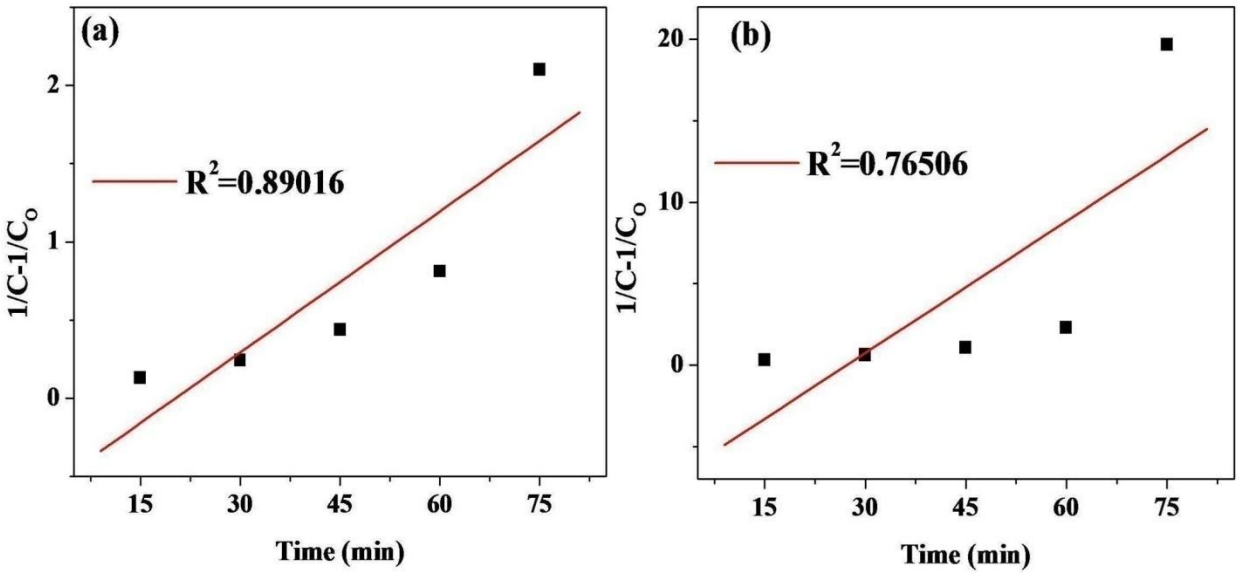


Fig.13 Pseudo-second order kinetics of (a) Undope NiO NPs (b) Ti-doped NiO NPs.

Antibacterial activity by well diffusion method

The antibacterial or antimicrobial activity of synthesized NiO and Ti-doped NiO nanoparticles is shown in Figures 14 and 15. It showed a larger zone of inhibition against bacteria that are harmful to humans, such as Klebsielilla pneumonia and Escherchia coli. Four distinct concentrations of each NiO and Ti doped NiO nanoparticle were used: 25 µL, 50 µL, 75 µL, and 100 µL, in order to either kill or inhibit the growth of bacteria (Lbeigi et al., 2019; Asefa et al., 2024). These synthesized NiO and Ti doped NiO nanoparticles greatly enhanced the antibacterial observation against these harmful bacteria. However, Ti doped NiO nanoparticles show a greater zone of inhibition than nickel oxide nanoparticles due to their smaller size and capacity to penetrate agar (Jirapat et al., 2016; Albokheet et al., 2021). Previous studies have reported the antibacterial effectiveness of Ti-doped NiO nanoparticles and the greatest zone of inhibition for NiO nanoparticles against E. coli (Dong et al., 2019). The bacterial cell dies or its growth is impeded because of the attachment of nanoparticles to its plasma membrane, or more precisely, to the protein that is present in the bacterial cell's plasma membrane. Transport across the plasma

membrane is significantly impacted by this connection (Chaudhary et al., 2019; Prasad & Swamy 2013). The zone of inhibition exhibited by NiO and Ti doped NiO is shown in figures 16 and 17.

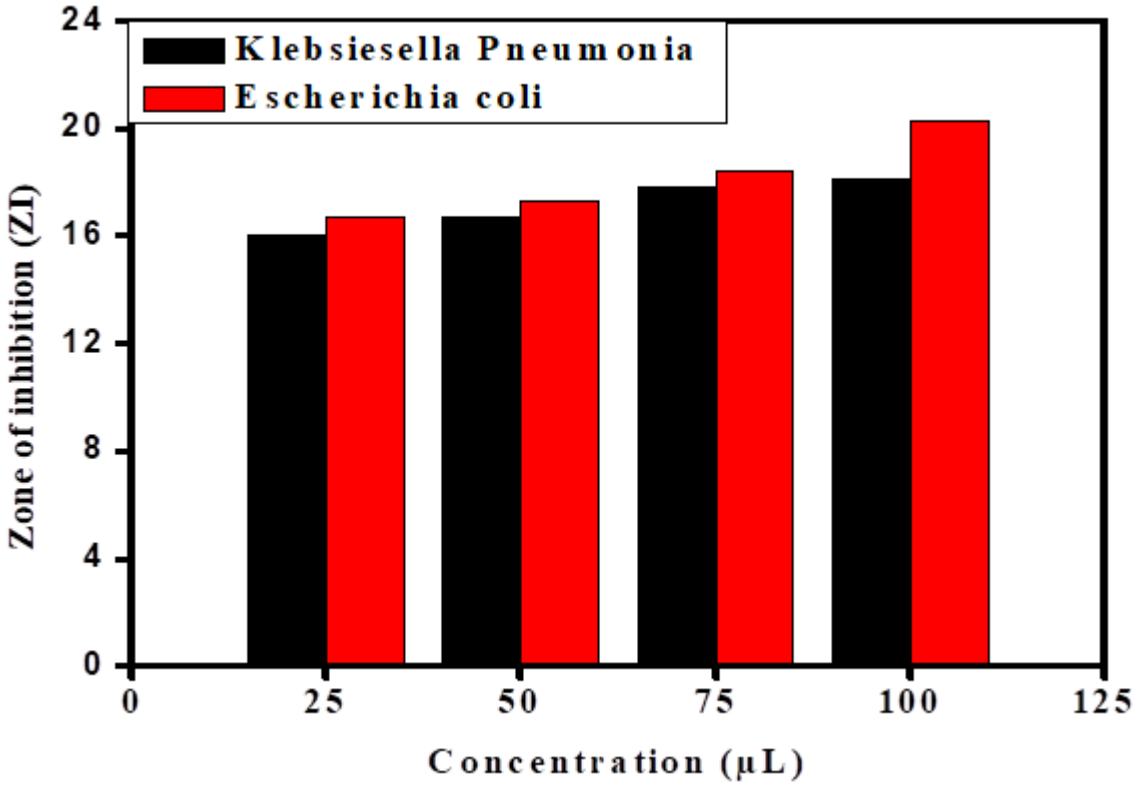


Fig. 14 Anti bacterial activity of NiO NPs.

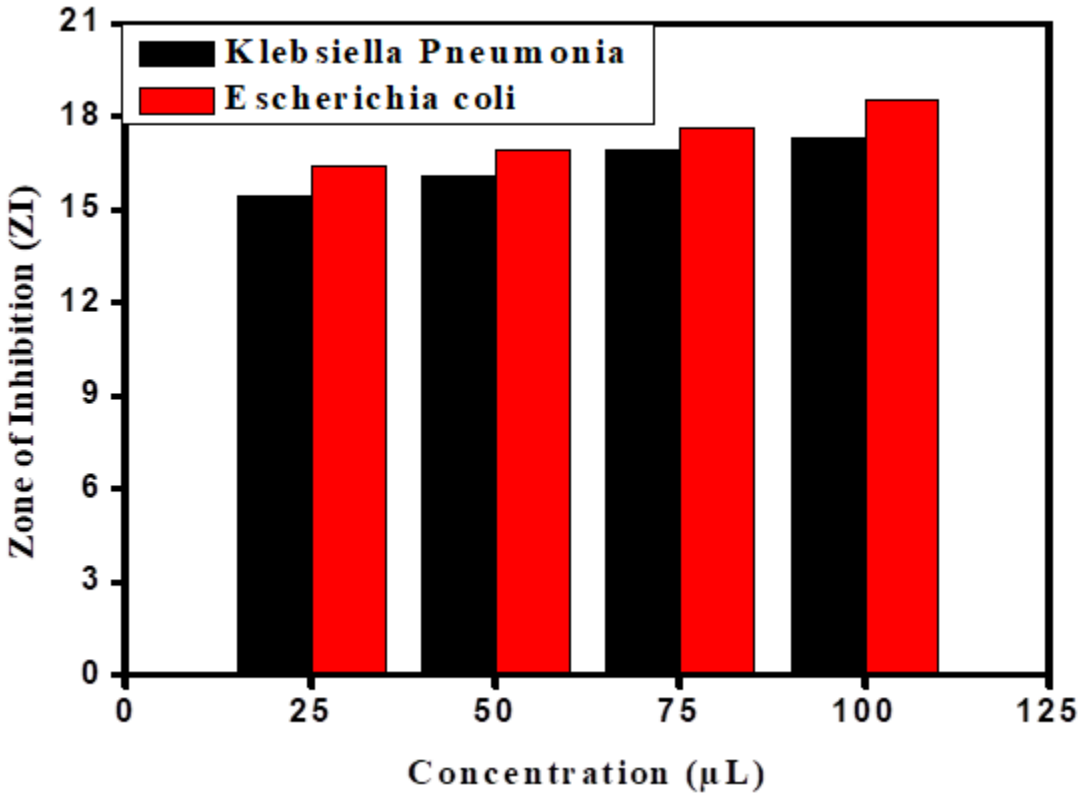


Fig. 15 Anti bacterial activity of Ti doped NiO NPs.

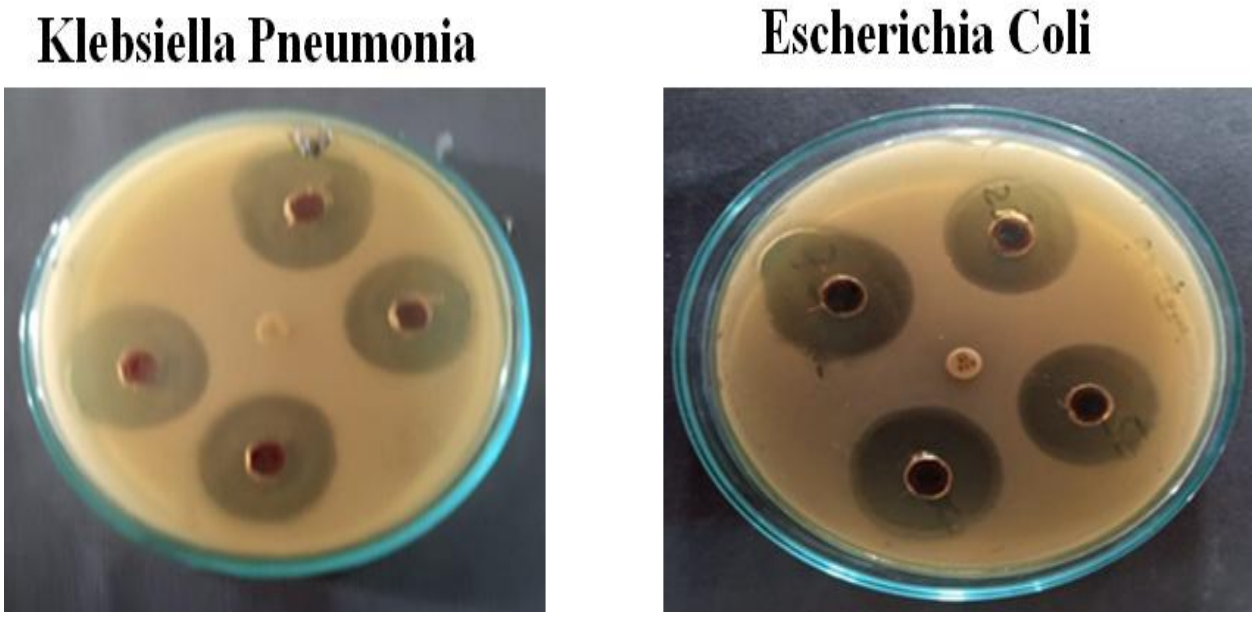


Figure 16 zone of inhibition show by NiO NPs.

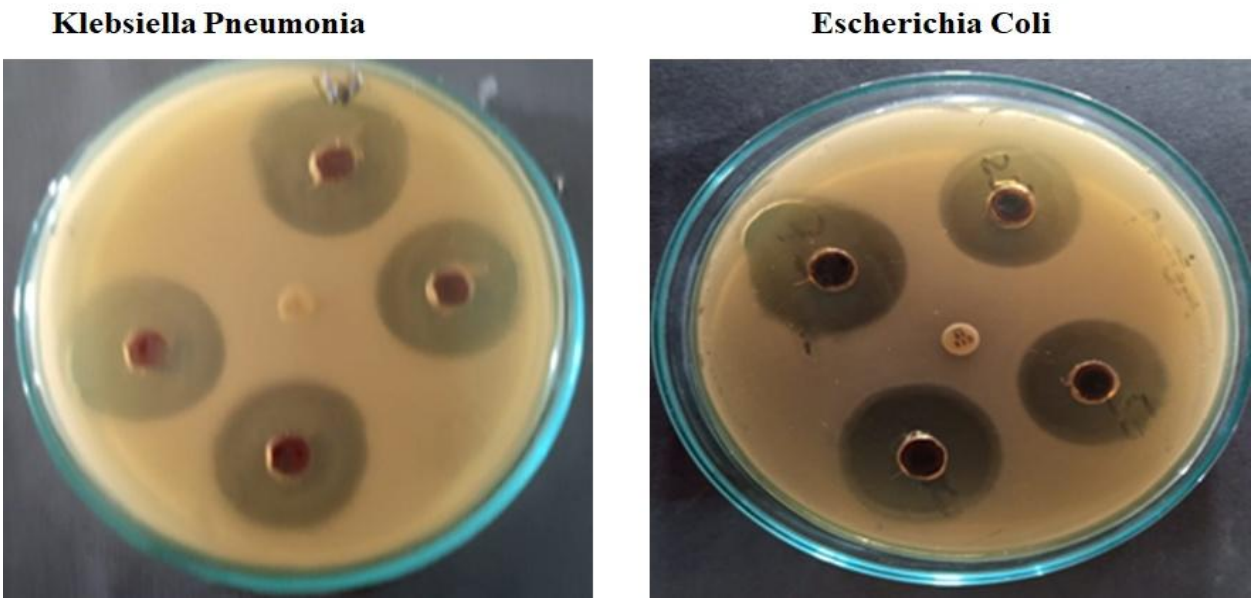


Fig. 17 zone of inhibition show by Ti doped NiO NPs.

Conclusion

In this study the NiO NPs and Ti doped NiO NPs were prepared using co-precipetation method. SEM illustrates that NiO has aggregated rough surface morphology while Ti doped NiO NPs had agglomerated and well dispersed. EDX and XRD confirm the better elemental composition and NPs size in nm rang. The optical band gap of Titanium doped Nickel oxide was smaller than NiO NPs. The prepared both NPs were used as catalysts for photodegradation of EY dye in aqueous medium. Various parameters were examined in this research like irradiation time, dosage of catalyst, pH study, recycling catalyst capability and initial dye concentration. It was concluded that as increasing irradiation time, the photocatalytic degradation of dye also increased. NiO and Ti doped NiO NPs degraded 84 and 96 percent dyes in 75 minute of time, respectively. The EY dye was also degraded by recovered NiO and Ti doped NiO NPs up to some extent. In photodegradation study, kinetic study demonstrates that EY dye degradation study obey Pseudo-first order kinetics. NiO NPs and Ti doped NiO NPs also exhibit antibacterial activity.

Funding

This study received no funding.

Data Availability

The authors declare that the data supporting the findings of this study are available within the paper.

Declarations

Conflict of interest

The authors declare no conflict of interest.

References

Kumari A, Sudesh KY (2014) Nanotechnology in agri-food sector. Crit Rev Food Sci 54:975-984.

Zhang L, Webster TJ (2009) Nanotechnology and nanomaterials: Promises for improved tissue regeneration. Nano Today4:66-80.

Hosein H-A, Strongin DR, Allen M et al (2004) Iron and cobalt oxide and metallic nanoparticles prepared from ferritin. Langmuir20: 10283-10287.

Saeed K, Zada N, Khan I et al (2019) Photocatalytic degradation of alizarin red dye in aqueous medium using carbon nanotubes/Cu–Ti oxide composites. Sep SciTechnol 54:2729–2737.

Kinkennon AE, Green DB, Hutchinson B (1995) The use of simulated or concentrated natural solar radiation for the TiO_2-mediated photodecomposition of basagran, diquat, and diuron, Chemosphere 31:8663–8671.

395 Chen SF, Mengyue Z, Yaowu T(1996) Photocatalytic degradation of organophosphorous
396 pesticides using TiO2 supported on fiberglass.JMicrochem 54:54–58.
397 Mehrazar E, Rahaie M, Rahaie S (2015) Application of nanoparticles for pesticides, herbicides,
398 fertilisers and animals feed management. Int J Nanoparticle 8:1-19.
399 Wei L, Shifu C, Wei Z, et al (2009) Titanium dioxide mediated photocatalytic degradation of
400 methamidophos in aqueous phase. J Hazard Mater164:154-160.
401 Deka AC, Sinha KS (2015) Mycogenic silver nanoparticle biosynthesis and its pesticide
402 degradation potentials. Int J TechnolEnhancEmergEng Res3: 108-113.
403 Kim T-S, Jung K-K, Kyungho Cet al (2006) Degradation mechanism and the toxicity assessment
404 in TiO_2 photocatalysis and photolysis of parathion. Chemosphere62:926-933.
405
406 Moza PN, Hustert K, Pal S et al (1992) Photocatalytic decomposition of pendimethalin and
407 alachlor. Chemosphere 11:1675-82.
408 Chandrasekaran K, Varaprasad K, Venugopal SK et al (2020) Synergistic antibacterial effect of
409 the magnesium-doped ZnO nanoparticles with chloramphenicol. Bio Nano Sci10:106-
410 111.
411 Dobrozhan O, Diachenkoa O, Kolesnyka M, et al (2019) Morphological, structural and optical
412 properties of Mg-doped ZnO nanocrystals synthesized using polyol process. Mat
413 SciSemiconProc102:590-595.
414 Buazar F, Bavi M, Kroushawi F et al(2016) Potato extract as reducing agent and stabiliser in a
415 facile green one-step synthesis of ZnO nanoparticles. J ExpNanosci11:175-184.
416 Khan SH, Pathak B (2020) Zinc oxide based photocatalytic degradation of persistent pesticides:
417 A comprehensive review. Environ Nanotech Mon Man 13:275-290.

Riyas ZM, Gayathri R, Prabhu MR et al (2022) Green synthesis and biomedical behavior of Mg-doped ZnO nanoparticle using leaf extract of Ficusreligiosa. Ceram Int 48:24619-24628.

Umaralikhan L, Jaffar MJ (2017) Green synthesis of ZnO and Mg doped ZnO nanoparticles and its optical properties. J Mater Sci: Mater Electron 28:7677-85.

Jayarambabu N, Kumari BS, Rao KV et al (2015) Beneficial role of zinc oxide nanoparticles on green crop production. Int J MultidiscipAdv Res Trends2: 273-82.

Kasi G, Viswanathan K, Sadeghi K et al(2019) Optical, thermal, and structural properties of polyurethane in Mg-doped zinc oxide nanoparticles for antibacterial activity. Prog Org Coat1: 309-315.

Muhammad W, Ullah N, Haroon M et al (2019) Optical, morphological and biological analysis of zinc oxide nanoparticles (ZnO NPs) using Papaver somniferum L. RSC Adv 9: 29541.

Kasi G, Viswanathan K, Seo J (2019) Effect of annealing temperature on the morphology and antibacterial activity of Mg-doped zinc oxide nanorods. Ceram Int 15: 3230-3238.

Aga KW, Efa MT, Beyene TT et al (2022) “Effects of Sulfur Doping and Temperature on the Energy Bandgap of ZnO Nanoparticles and Their Antibacterial Activities” ACS Omega 7: 10796−10803.

Soosen MS, Bose L, George KC et al (2009) Optical properties of zno nanoparticles. ISSN 1: 57-65.

Naz F, Saeed K (2021) Investigation of photocatalytic behavior of undoped ZnO and Cr-doped ZnO nanoparticles for the degradation of dye. Inorg. Nano-Metal Chem 51: 1-11.

Sivagami K, Vikraman B, Krishna RR, et al (2016) Chlorpyrifos and endosulfan degradation studies in an annular slurry photo reactor. Ecotox Environ Safe.134:327-331.

Khairnar SD, Shrivastava VS (2019) Photocatalytic degradation of chlorpyrifos and methylene blue using α-Bi_2O_3 nanoparticles fabricated by sol–gel method. SN ApplSci1:1-10.

Sauer T, Neto G. C, Jose H. J, Moreira R et al (2022) "Kinetics of photocatalytic degradation of reactive dyes in a TiO2 slurry reactor" J. Photochem. Photobiol. A. Chem., 149, 147–154. Chakrabarti S, Dutta B.K (2004) "Photocatalytic degradation of model textile dyes in wastewater using ZnO as semiconductor catalyst" J. Hazard. Mater., 92, 700- 709.

Khan I, Saeed K, Zekker I, Zhang B, Hendi A. H, Ahmad A, Ahmad S, Zada N, Ahmad H, Shah L. A, Shah T, Khan I et al (2022) Review on Methylene Blue: Its Properties, Uses, Toxicity and Photodegradation. Water 2022, 14, 1-30.

Michael, CA., Dominey-Howes D, Labbate D (2014) The antimicrobial resistance crisis: causes, consequences, and management. Front Public Health, **2**:145.

Xie Y, He Y, Irwin PL et al(2011) Antibacterial activity and mechanism of action of zinc oxide nanoparticles against *Campylobacter jejuni*. Appl Environ Microbiol**77**: 2325–2331.

Azam A, Ahmed AS, Oves M et al (2012) Size-dependent antimicrobial properties of CuO nanoparticles against Gram -positive and -negative bacterial strains. Int J Nanomed**7**:3527-3535.

Ribeiro JBP, Miranda-Vilela AL, Graziani et al (2016) Evaluation of the efficacy of systemic miltefosine associated with photodynamic therapy with liposomal chloroaluminiumphthalocyanine in the treatment of cutaneous leishmaniasis caused by Leishmania (L.) amazonensis in C57BL/6 mice.Photodiagnosisphotodynther 13:282-290.

Sergiev I, Todorova D, Shopova E, Jankauskiene J, Jankovska-Bortkevic E, Jurkoniene S et al (2019) Exogenous auxin type compounds amend PEG-induced physiological responses of pea plants. Sci Hortic 248:200-205.